LHCb-ANA-2012-105
Draft 2b, November 21, 2012

First Observation of the Double Cabbibo forbidden decay $\Lambda_c \to pK^+\pi^-$ with the 2011 data

T. Ruf[1]

[1] *European Organization for Nuclear Research (CERN), Geneva, Switzerland*

Abstract

This note presents an analysis of the double Cabbibo suppressed decay of $\Lambda_c{}^+ \to pK^+\pi^-$using charm produced in semileptonic B-decays. This decay had not been observed so far, the PDG(2012) quotes an upper limit of the branching ratio of $< 2.3 \times 10^{-4}$ at 90% CL. The analysis uses the full statistics of 2011 data, $\approx 1\text{fb}^{-1}$, from the stripping 17b semileptonic stream. A clear signal of 568 ± 59 events is observed, compared to $(336.7 \pm 0.7) \times 10^3$ Cabbibo favoured decays, resulting in a branching ratio of $(8.2 \pm 0.9_{\text{stat.}} \pm 0.6_{\text{sys.}} \pm 2.2_{\text{pdg}}) \times 10^{-5}$. In addition, estimates of $\Lambda_c{}^+ \to pK^+K^-$and $\Lambda_c{}^+ \to p\pi^+\pi^-$event yields using the semileptonic stream are given in an Appendix.

Changes:

- 21/11/2012: Adding results for acceptance/charge symmetrized pKpi combinations
- 5/11/2012: Trying to incorporate comments of Mat Charles:

  Correction factors applied to final DCS/CF result. PID correction factor has a slight dependence on Dalitz plot representation. Use largest deviation from unity as systematic error.

  Added plot of decaylength and KK mass following questions during review

  Added axis labels

  Moved pKK and p$\pi\pi$ to Appendix.

- 10/10/2012:

  Added study of angular distributions for the CF and DCS mode

  Study of possible reflections due to particle mis-identification

- 19/9/2012: New microDST production finished. Due to previous technical problems, now, statistics increased by 30%. Change of analysis strategy:

  Move to well defined trigger lines and only accept L0-HLT1-HLT2 TOS events

  Check sign of muon against sign of proton, and only accept right sign combinations also for KK and $\pi\pi$ modes.

  Added background free Dalitz plots

  Study of efficiencies over Dalitz plot

- 6/8/2012: accidentally, PID cut only applied to one pion in $\pi^+\pi^-$ mode. Corrected, reduces yield by 17%.
- 2/8/2012: added results for TOS events as cross check. Added wrong tag events to CF mode when making ratios SCS/CF, 0.5% correction.
- 31/7/2012: Cuts on $p_T(\mu) > 1.8\,\mathrm{GeV}/c$ and $\Delta z > 0$ were missing for the p$\pi^+\pi^-$ and pKK modes, resulting in too large yields with respect to the CF mode. Fixed, Table and Figure updated. Thanks to Patrick Spradlin for noticing the issue with the yields.

Contents

1 Overview of the Note

This note presents an analysis of the double Cabbibo suppressed decay (DCS) of $\Lambda_c^+ \to pK^+\pi^-$using charm produced in semileptonic B-decays. This decay had not been observed so far, the PDG(2012) quotes an upper limit of the branching ratio of $< 2.3\times10^{-4}$ at 90% CL. The tree diagrams for the Cabbibo favoured decay (CF) and the DCS decay are shown in Fig.1. Naively, one would expect a ratio of branching ratios of 0.3% for DCS/CF mode. This works fine for $D^0 \to K^+\pi^-$, but fails for other examples.

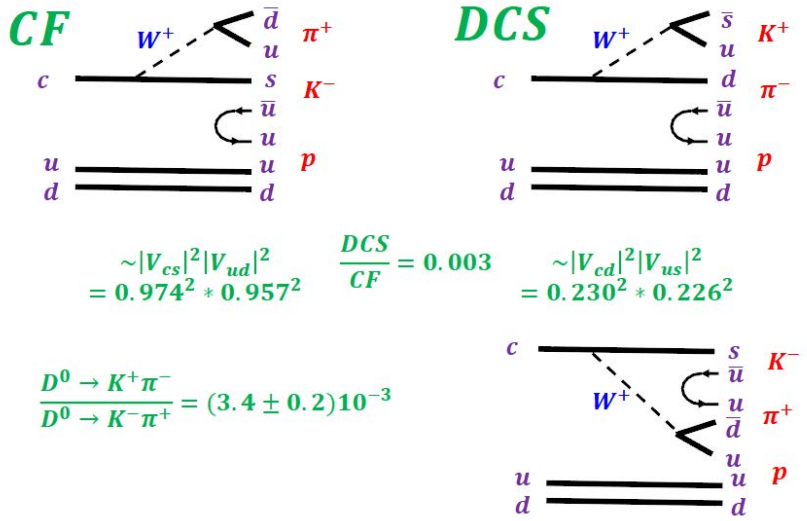

Figure 1: Leading Feynman diagrams.

The analysis uses the full statistics of 2011 data, 1.1fb^{-1}, from the stripping 17b semileptonic stream. A clear signal of 568 ± 59 events is observed, compared to $(336.7 \pm 0.7) \times 10^3$ Cabbibo favoured decays, resulting in a branching ratio of $(8.2 \pm 0.9_{\text{stat.}} \pm 0.6_{\text{sys.}} \pm 2.2_{\text{pdg}}) \times 10^{-5}$. The note describes the cuts used in the stripping, the analysis procedure and discusses the systematic errors. During this analysis, as a byproduct, also the $\Lambda_c^+ \to pK^+K^-$and $\Lambda_c^+ \to p\pi^+\pi^-$decay modes using the semileptonic stream were looked at. For future reference, the results obtained so far for these decay modes are summarized in Appendix 7.

Throughout the note, the charged conjugated state are always included in the plots and results, e.g. $\Lambda_c^+ \to pK^-\pi^+ = \Lambda_c^+ \to pK^-\pi^+ + \Lambda_c^- \to \bar{p}K^+\pi^-$.

2 Selections

2.1 Stripping 17b, Semileptonic Stream

In Table 1 the cuts which are applied in stripping 17b are shown.

Table 1: Cuts of stripping 17b

For Protons, Kaons	and Pions
TrackChi2	< 4
P	$> 2\,\mathrm{GeV}/c$
$\mathrm{P_T}$	$> 300\,\mathrm{MeV}/c$
MinIPChi2	> 9
For Protons only	
StdLooseProtons	
dllP	> 4
dllP-dllK	> 0
For Kaons only	
StdLooseKaons	
dllK	> 4
For Pions only	
StdLoosePions	
dllK	< 10
For Muons	
StdLooseMuons	
TrackChi2	< 5
P	$> 3\,\mathrm{GeV}/c$
$\mathrm{P_T}$	$> 800\,\mathrm{MeV}/c$
MinIPChi2	> 4
dllmu	> 0
For Λ_c	
Mass window	100 MeV
$\mathrm{SumP_T}$	$> 1800\,\mathrm{MeV}/c$
ADOCACHI2CUT	20
VFASPF(VCHI2/VDOF)	< 6
BPVVDCHI2	> 100
BPVDIRA	> 0.99
For "B"	
AM	$< 6.2\,\mathrm{GeV}$
MM	[2.5, 6.0] GeV
VFASPF(VCHI2/VDOF)	< 6
BPVDIRA	> 0.999

2.2 Offline Cuts

Since the event yield of the Cabbibo suppressed decay (DCS) is measured relative to the Cabbibo favoured (CF) mode, and the particles in the final state are identical, it is expected that the trigger and reconstruction efficiencies cancel in first order. Basics cuts,

see Table 2, Fig.2 and Fig.3, exploring the semileptonic B-decay kinematics and particle identification, inspired from the semileptonic deltaACP analysis[1], are used to remove efficiently the background events.

Table 2: Offline cuts

$P_T(\mu)$	$> 1.8\,\text{GeV}/c$
$P_T(\Lambda_c)$	$> 1.5\,\text{GeV}/c$
B-mass	[3.5, 5.3] GeV
CF: charge(K)×charge(μ)	> 0
DCS: charge(K)×charge(μ)	< 0
VZ(Λ_c)-VZ(B)	> 0
dllP(p)-dllK(p)	> 10
dllK(K)	> 10
dllK(π)	< -5
TOS events	L0MuonDecision for the muon candidate, Hlt1TrackAllL0Decision or Hlt1TrackMuonDecision and Hlt2TopoMuNBodyBBDTDecision or Hlt2SingleMuonDecision

Specific for charm produced in semileptonic B decays are the cuts on the charge of the muon compared to the charge of the kaon, which in case of DCS reduces a lot the combinatorics arising from normal $b \to c \to s$ transitions, and on the pseudo B-mass, Fig.3. Fig.4 shows the decay length distribution for $pK^-\pi^+$ combinations in signal region and lower mass sideband. The decay length of the background is in general larger than for signal, indicating that the background originates mainly from charm hadron decays, and not from "prompt" B decay products. Requiring a larger displacement than $VZ(\Lambda_c) - VZ(B) > 0$ would not improve the signal over background ratio.

The TISTOS tools are used, requiring L0MuonDecision for the muon candidate (=L0MuonTOS), Hlt1TrackAllL0Decision or Hlt1TrackMuonDecision (=HLT1TOS) and Hlt2TopoMu(2,3,4)BodyBBDTDecision or Hlt2SingleMuonDecision (=HLT2TOS) for the B candidate.

2.2.1 Yields

The invariant mass distributions are fitted with a double gaussian for the signal and a polynomial of first order for the background. The widths, central values and the relative contribution of the two gaussians are obtained from the fit to the CF decays and fixed in the fit to the DCS decays. The fitted mass distributions are shown in Fig.5. Fit parameters are given in Table 3. Fit results for events without TOS requirement are given in Appendix II. It is noted that the yields for all pHH modes are reduced by about 10% when requiring TOS.

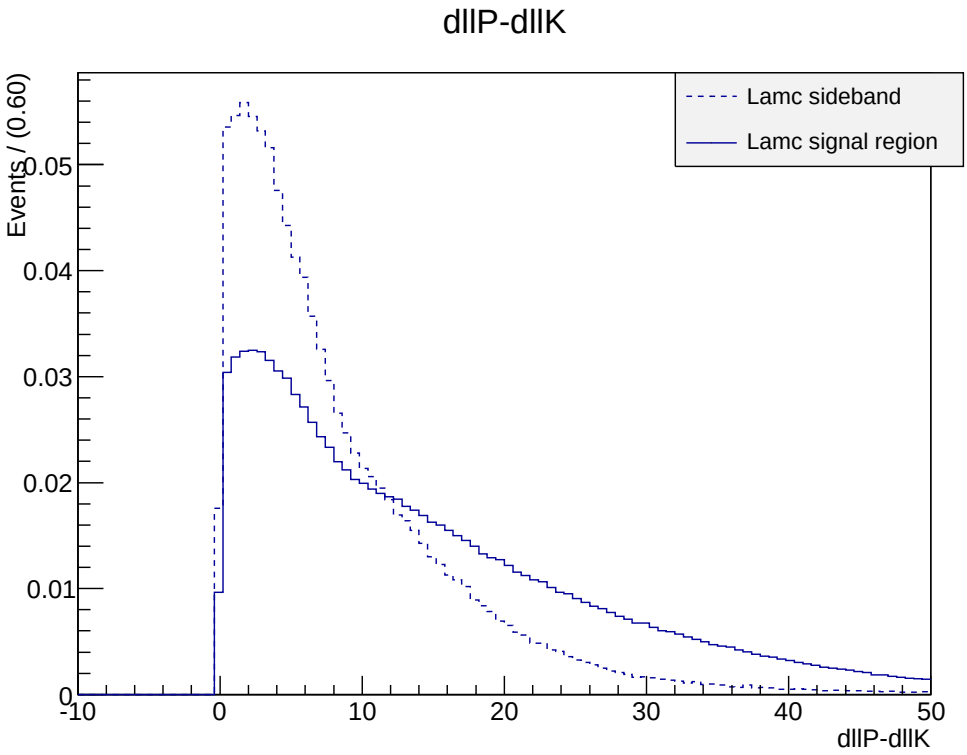

Figure 2: The dll(p)-dll(K) distribution for $pK^-\pi^+$ combinations in signal region and lower mass sideband.

The fitted yields are $(336.7 \pm 0.7) \times 10^3$ CF decays and 568 ± 59 DCS decays, resulting in a raw ratio DCS/CF of $(1.69 \pm 0.18) \times 10^{-3}$. The mistag rate, decays with a wrong charge of the muon compared to the charge of the proton, of $\omega =\approx 0.5\%$ is compatible with the rates measured in the deltaACP analysis using D-meson decays ($\omega =\approx 1\%$), although a bit lower. Within the statistical error, the measured mistag rate for the DCS decays, $\omega = (23 \pm 12)\%$ is in agreement with the expectation.

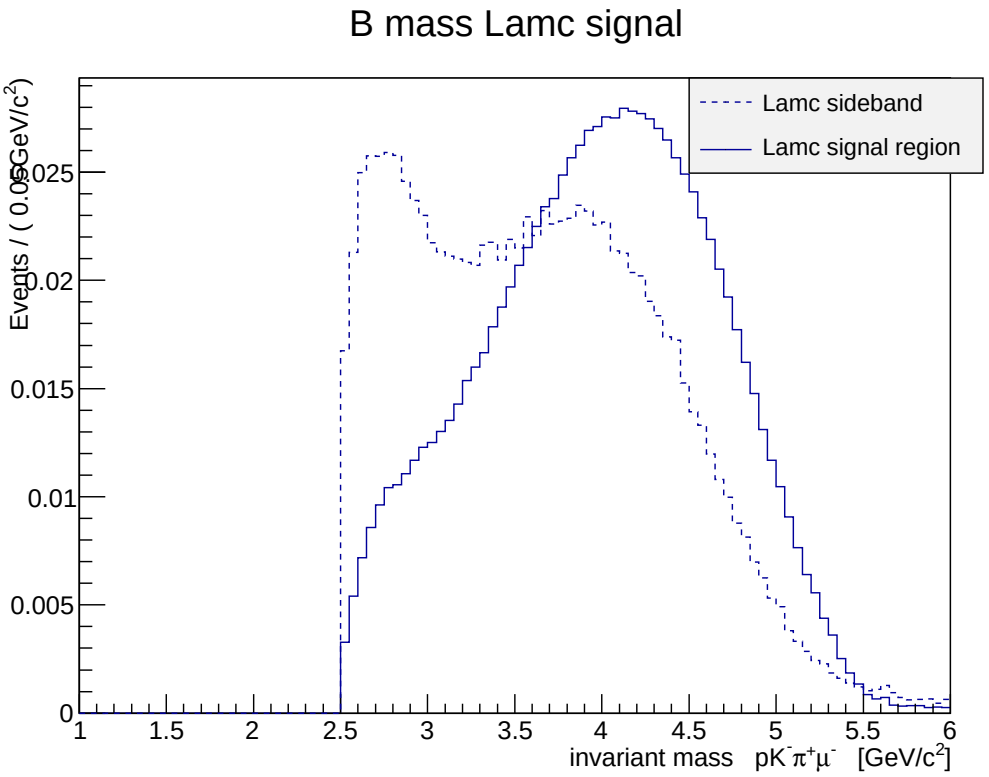

Figure 3: The invariant mass distribution for $pK^-\pi^+\mu^-$ combinations in signal region and lower mass sideband.

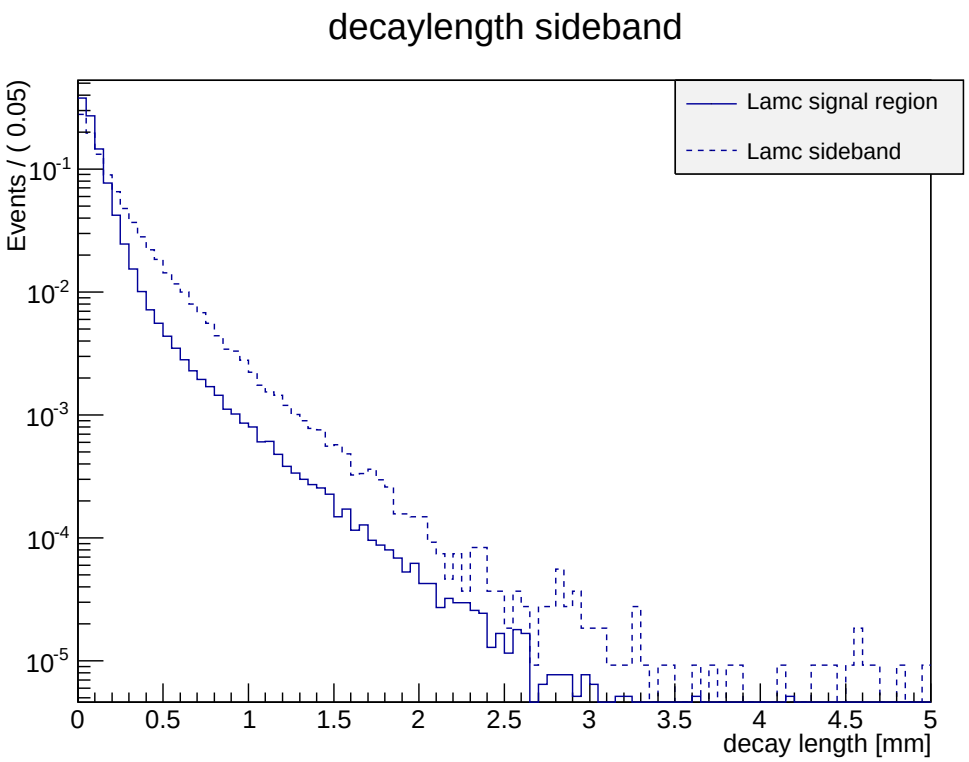

Figure 4: The decay length distribution for $pK^-\pi^+$ combinations in signal region and lower mass sideband.

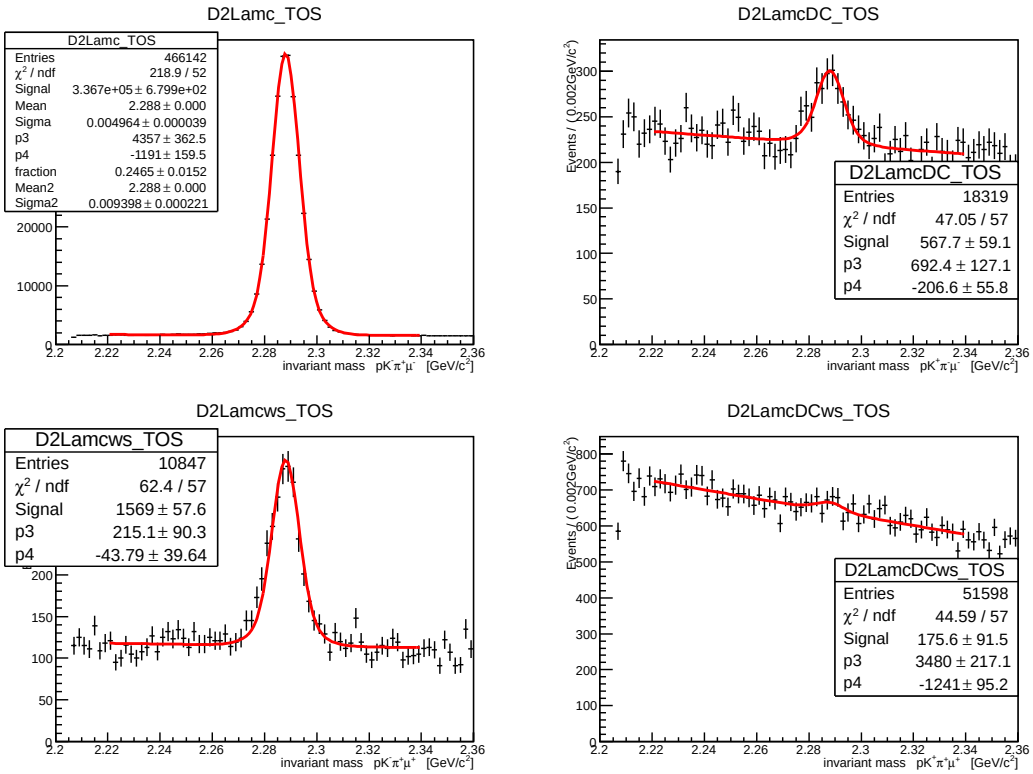

Figure 5: TOS events, the invariant mass distribution is shown for $pK^-\pi^+\mu^-$, CF, top left, $pK^+\pi^-\mu^-$, DCS, top right, $pK^-\pi^+\mu^+$, CF wrong sign μ, bottom left and $pK^+\pi^-\mu^+$, DCS wrong sign μ, bottom left.

Table 3: Fit parameters of the mass fits separately for magnet up and down, Λ_c^+ and Λ_c^-, for L0 and HLT TOS events.

Fit parameter	All	Magnet up	Magnet down	Λ_c^+	Λ_c^-
n_{CF}	336661.6 ± 679.9	139457.6 ± 438.8	197221.1 ± 519.5	165690.3 ± 496.5	171143.9 ± 474.5
$mean_1$	2.28807 ± 0.00002	2.28814 ± 0.00003	2.28803 ± 0.00002	2.28810 ± 0.00002	2.28805 ± 0.00002
$mean_2$	2.28811 ± 0.00007	2.28816 ± 0.00012	2.28807 ± 0.00009	2.28811 ± 0.00013	2.28810 ± 0.00009
σ_1	0.00496 ± 0.00004	0.00498 ± 0.00006	0.00495 ± 0.00005	0.00508 ± 0.00005	0.00486 ± 0.00006
σ_2	0.00940 ± 0.00022	0.00948 ± 0.00036	0.00935 ± 0.00028	0.01024 ± 0.00041	0.00889 ± 0.00025
ratio	0.25 ± 0.02	0.24 ± 0.02	0.25 ± 0.02	0.20 ± 0.02	0.29 ± 0.02
n_{DCS}	567.7 ± 59.1	278.7 ± 38.7	285.4 ± 44.6	265.3 ± 40.8	299.8 ± 42.7
$n_{DCS}/n_{CF}[10^{-3}]$	1.69 ± 0.18	2.00 ± 0.28	1.45 ± 0.23	1.60 ± 0.25	1.75 ± 0.25

Table 4: Fit parameters of the mass fits separately for magnet up and down, Λ_c^+ and Λ_c^-, for L0 and HLT TOS events with acceptance requirement on charge conjugated states for kaon and pion.

Fit parameter	All	Magnet up	Magnet down	Λ_c^+	Λ_c^-
n_{CF}	319992.3 ± 660.6	132553.1 ± 426.2	187455.2 ± 504.8	157656.5 ± 482.2	162501.1 ± 461.1
$mean_1$	2.28807 ± 0.00002	2.28813 ± 0.00003	2.28803 ± 0.00002	2.28809 ± 0.00002	2.28805 ± 0.00003
$mean_2$	2.28809 ± 0.00007	2.28813 ± 0.00012	2.28805 ± 0.00009	2.28807 ± 0.00013	2.28809 ± 0.00009
σ_1	0.00495 ± 0.00004	0.00496 ± 0.00006	0.00494 ± 0.00005	0.00506 ± 0.00005	0.00486 ± 0.00006
σ_2	0.00935 ± 0.00022	0.00941 ± 0.00036	0.00930 ± 0.00028	0.01016 ± 0.00041	0.00886 ± 0.00025
ratio	0.25 ± 0.02	0.24 ± 0.02	0.25 ± 0.02	0.20 ± 0.02	0.29 ± 0.02
n_{DCS}	539.4 ± 56.7	256.9 ± 37.0	279.3 ± 42.9	241.1 ± 39.0	297.7 ± 41.1
$n_{DCS}/n_{CF}[10^{-3}]$	1.69 ± 0.18	1.94 ± 0.28	1.49 ± 0.23	1.53 ± 0.25	1.83 ± 0.25

2.3 Reflections

The question, "Can the DCS signal peak be due to reflections of the CF mode or D_s decays caused by particle misidentification ?", had been studied by taking the events around the observed CF and DCS mass peaks, $\pm 2\sigma$, and changing the mass assignments. The following cases are studied, double misidentification $K \to \pi$ and $\pi \to K$ would cause feedthrough from CF mode, $\pi \to K$ and $\pi \to K$ would cause feedthrough from D_s and triple misidentification $p \to K$, $K \to \pi$ and $\pi \to K$ also feedthrough from D_s. No significant peaks are observed, see Fig.6, except of a small excess around the D_s mass in case of misidentifying two kaons as a proton and a pion for the DCS mode. There is no excess seen in the Λ_c sidebands, or for the CF mode. If the excess is fitted with a gaussian of expected width and mean value for $D_s \to KKK$, a signal of 21 ± 9 events is obtained. Looking at $D_s \to KKK$ prompt MC, Fig.7, and changing the mass assignments correspondingly, does not give any excess at the Λ_c mass. It is therefore assumed that the excess seen in Fig.6 is a statistical fluctuation.

Following a suggestion during the review, the invariant mass distribution of $K^-\pi^+$ combinations when assigning the kaon mass to the pion candidate, Fig.8, had been studied to look for a Φ signal. No Φ signal is seen for the CF (top) and for the DCS (bottom) mode.

is seen for the CF (top) and DCS (bottom) mode.

2.4 Investigation of possible acceptance differences for same and opposite charged kaon - proton combinations

This study is done using a data-driven approach. The first state of a kaon or pion is used to extrapolate to the different T station locations, and the trajectory is required to be in the acceptance at any T location. The same exercise is repeated by reverting the sign of the charge of the pion and kaon. In this way, the combinations $pK^-\pi^+$ and $pK^+\pi^-$ are symmetric with respect to the LHCb detector acceptance. The mass fit results are summarized in Table 4. About 5% of the events are being removed by this procedure, for the CF and DCS mode. There is essentially no change in the final result for the DCS/CF ratio measurement. No systematic error is being assigned.

2.5 Dalitz plots

The event yields are extracted from fits in bins of the $K\pi/\pi p$ dalitz plot (double gaussian for signal and polynomial first order for the background, for the DCS mode, the shape parameters are taken from the CF fit, only signal yield and background floating) and and then plotted in Fig.9 and Fig.10 together with the χ^2/dof of each of the fits. The individual fits for the DCS mode are shown in Fig.25.

Both decay modes show a clear K^* resonance contribution. Fig.11 shows the $K\pi$ mass against the $pK\pi$ mass, also showing the K^* resonance contribution.

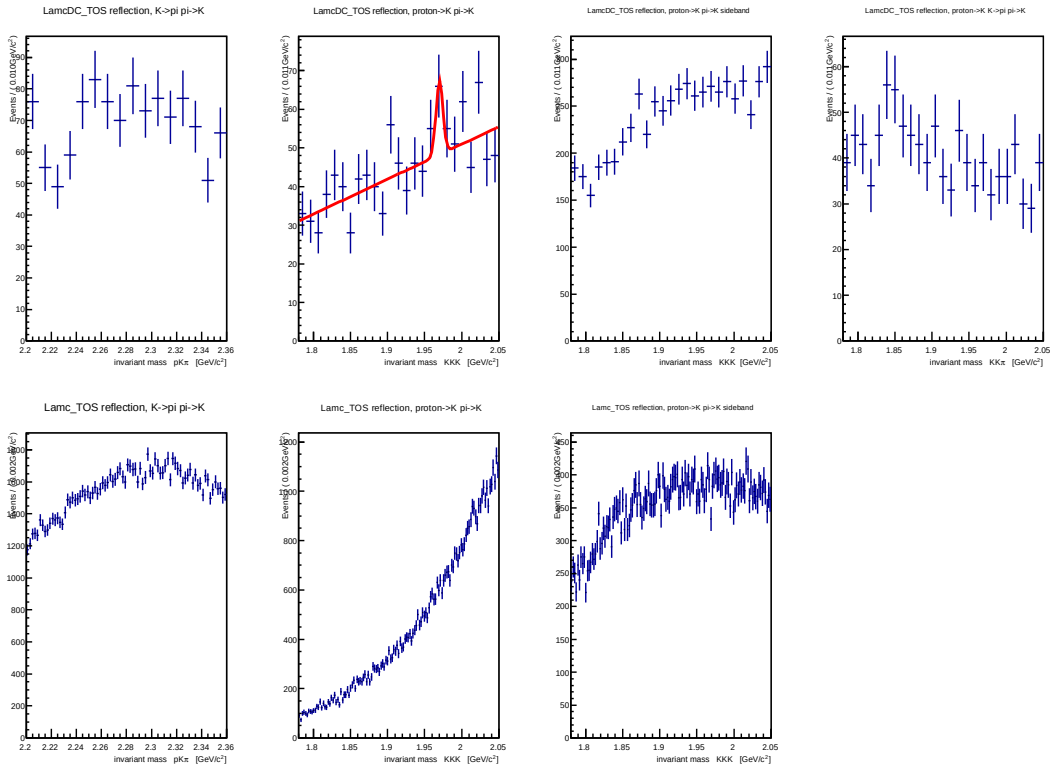

Figure 6: Invariant mass distributions with different mass assignments to search for reflections. Top: DCS mode, bottom: CF mode. From left to right: $K \to \pi$ and $\pi \to K$, $\pi \to K$ and $p \to K$ taking events from Λ_c signal region, $\pi \to K$ and $p \to K$ taking events from the Λ_c sidebands, $p \to K$, $K \to \pi$ and $\pi \to K$ taking events from Λ_c signal region for the DCS mode only.

The number of decays ${\Lambda_c}^+ \to pK^{*0}$and ${\Lambda_c}^+ \to p\overline{K}^{*0}$are obtained by plotting the number of events as function of the $pK\pi$ invariant mass in bins of the $K\pi$ mass, fitting for the Λ_c signal with a double gaussian and first order polynomial for the background, plotting the number of Λ_c events as function of $K\pi$ mass and fitting with a Breit-Wigner for the K^* signal and a second order polynomial for the non-resonant contribution, Fig.12. For the CF mode, the fitted mass and width, $m = (898.4 \pm 0.2)\,MeV/c^2$, $\Gamma = (51.8 \pm 0.9)\,MeV$, are in reasonable agreement with the PDG average values, $m = (895.94 \pm 0.22)\,MeV/c^2$ and $\Gamma = (48.7 \pm 0.8)\,MeV$. For the DCS mode, due to much lower statistics, the mass and width are constrained to the CF results.

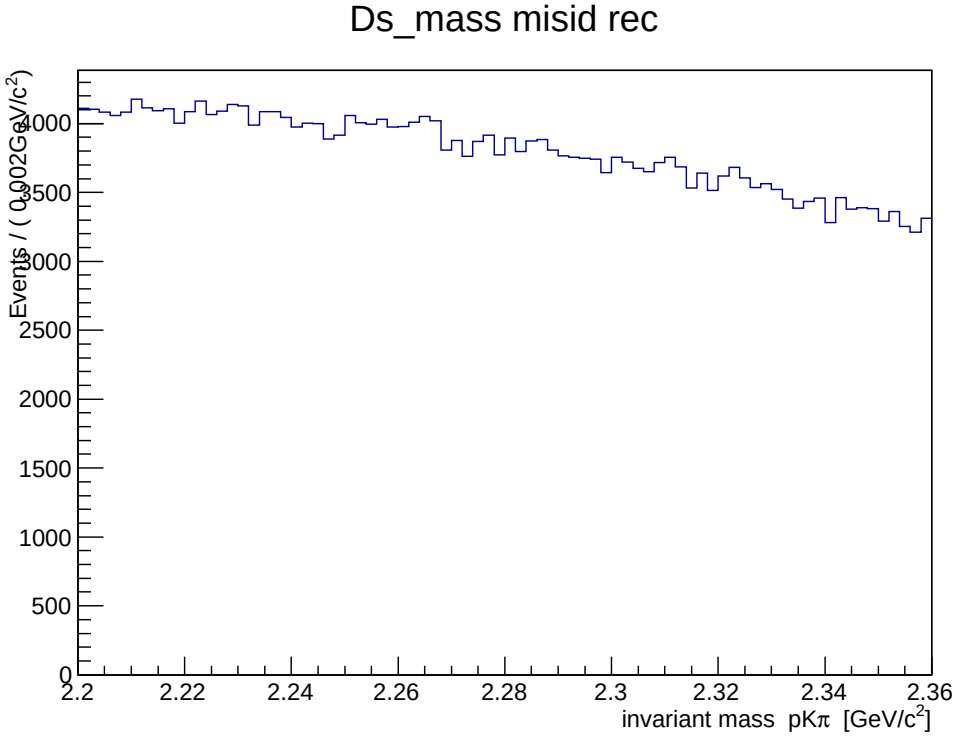

Figure 7: MC: Invariant mass distribution of $D_s \to KKK$ when changing $K \to \pi$ and $K \to p$.

Table 5: $\Lambda_c^+ \to pK^{*0}$and $\Lambda_c^+ \to p\overline{K}^{*0}$fit results.

mode	N
$\Lambda_c^+ \to pK^{*0}$	58574.6 ± 993.5
$\Lambda_c^+ \to p\overline{K}^{*0}$	397.7 ± 51.3
ratio	$(6.79 \pm 0.88) \times 10^{-3}$

3 MC Studies

3.1 Efficiencies across Dalitz plot

Fig.13 shows the MC Dalitz plots for generated (starting top left), reconstructed, stripped, offline selected and triggered events, together with the corresponding efficiency for each of the steps. The bottom left plot shows the total efficiency. It is noted that the MC generated Dalitz plot does not describe too well the data, Fig.9. However for the efficiency discussion in bins of the Dalitz plot, this is not important. The mean total efficiency averaged over the Dalitz plot is 0.31% with a variation of RMS= 0.1%.

Taking the MC efficiency in bins of the Dalitz plot and correcting the CF and DCS

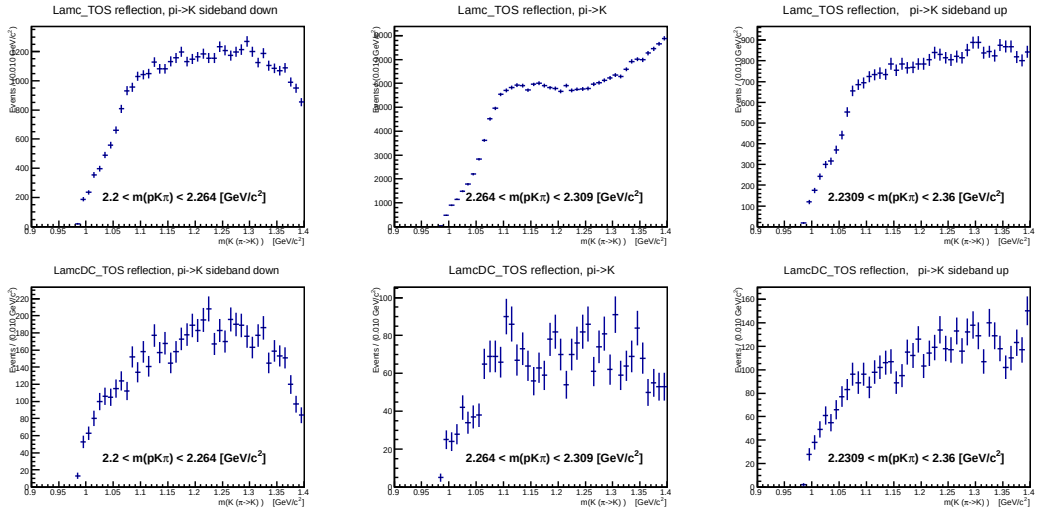

Figure 8: Invariant mass distribution of $K^-\pi^+$ combinations with assigning the kaon mass to the pion candidate. No Φ signal is seen for the CF (top) and DCS (bottom) mode.

data, results in an average efficiency for the CF mode of 0.293% and for the DCS mode of 0.295%, leaving essentially the raw ratio of CF/DCS unchanged.

3.2 Angular distributions and efficiencies, MC

Using the angles defined in Fig.14, except of replacing the beam direction with the Λ_b flight direction, the bias introduced in different steps of the reconstruction, tracking, stripping cuts, offline selection, trigger are shown in Fig.15, Fig.16 and Fig.17. On top are the actual distributions, for example top left at generator level, bottom row are the efficiencies of each step versus compared previous step. The total efficiency is shown in bottom left plot. One can see that the generated distributions are all flat, no polarizations. The detector acceptance and track reconstruction are causing the main distortions, while the offline selection and the trigger do not cause any significant bias as function of these variables, except for the particle ID cuts.

3.3 Comparison of angular distribution, data and MC

Fig.18 shows the same angular distributions for the CF and DCS decay, overlayed with the total MC efficiency. The agreement with the MC is very good for both modes, indicating that there are no sizeable polarizations in data. Fig.18 shows the same angular distributions cutting in the K^* mass region.

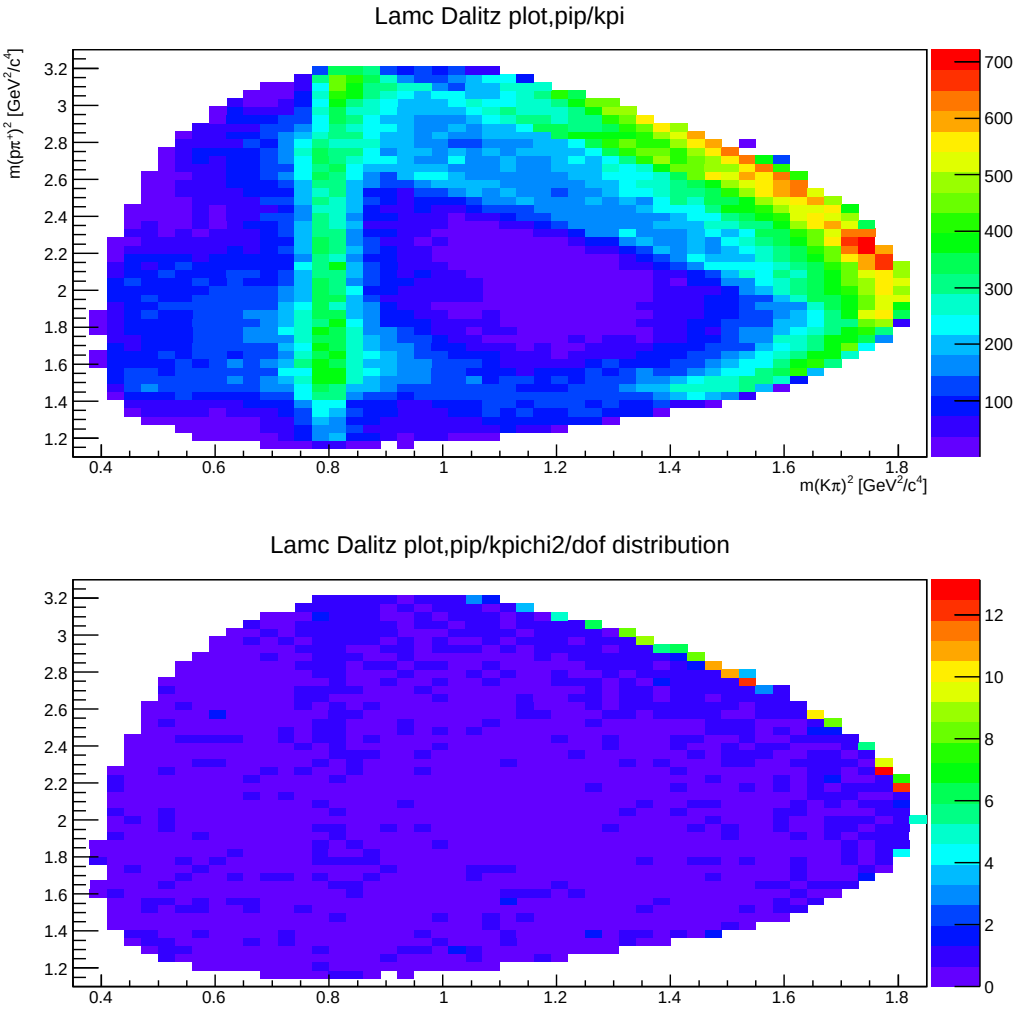

Figure 9: Dalitz plot for the CF.

3.4 PID efficiencies using the RICH Tables

Instead of using the MC, one can use PID efficiencies measured from data to evaluate possible differences between the efficiencies for the CF and DCS mode. Weighting events with PID efficiencies, and dividing number of weighted signal events by unweighted in bins of the Dalitz plot gives the distribution of mean PID efficiencies across the Dalitz plot, Fig.20 and Fig.21. For CF, one obtains a mean efficiency of 61.7% and for the DCS mode of 62.9% compared to the MC PID efficiency on TOS events of 57.3%. Using the other two different representations of the Dalitz plot, mean efficiencies of 62.3% and 61.6% for the CF mode and 64.5% and 64.5% for the corresponding DCS mode are obtained.

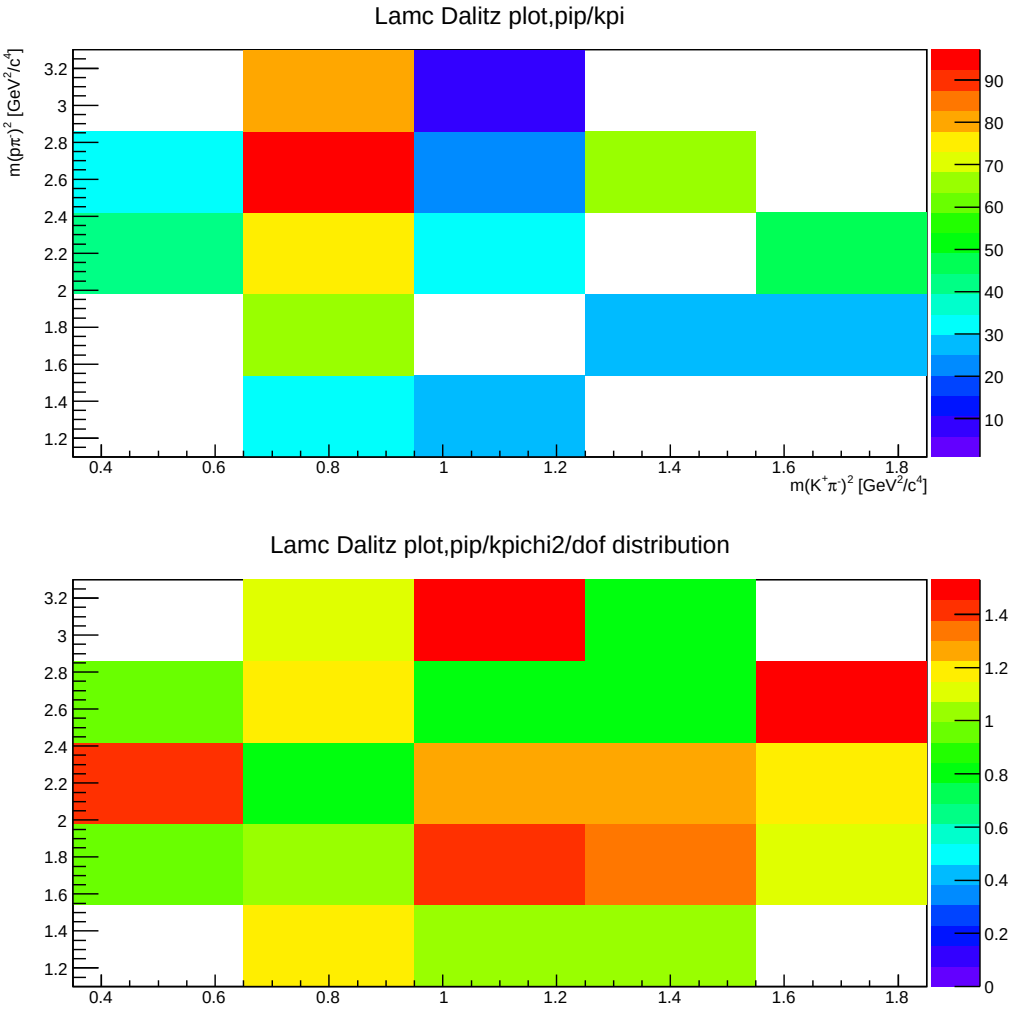

Figure 10: Dalitz plot for the DCS mode.

3.5 p_T distributions

A first look at the p_T distribution of the reconstructed Λ_c, Fig.22, does not show any significant difference between the CF and DCS mode, supporting the assumption that within present statistical errors, there is no difference in reconstruction efficiencies between the CF and DCS mode. Taking as an extreme case, adding up all the differences in the central values between the CF and DCS mode in Fig.22, ignoring the statistical errors, would result in a systematic error of 23%. A more realistic estimate, adding up only differences which are larger than the statistical error, results in a systematic error of 5%.

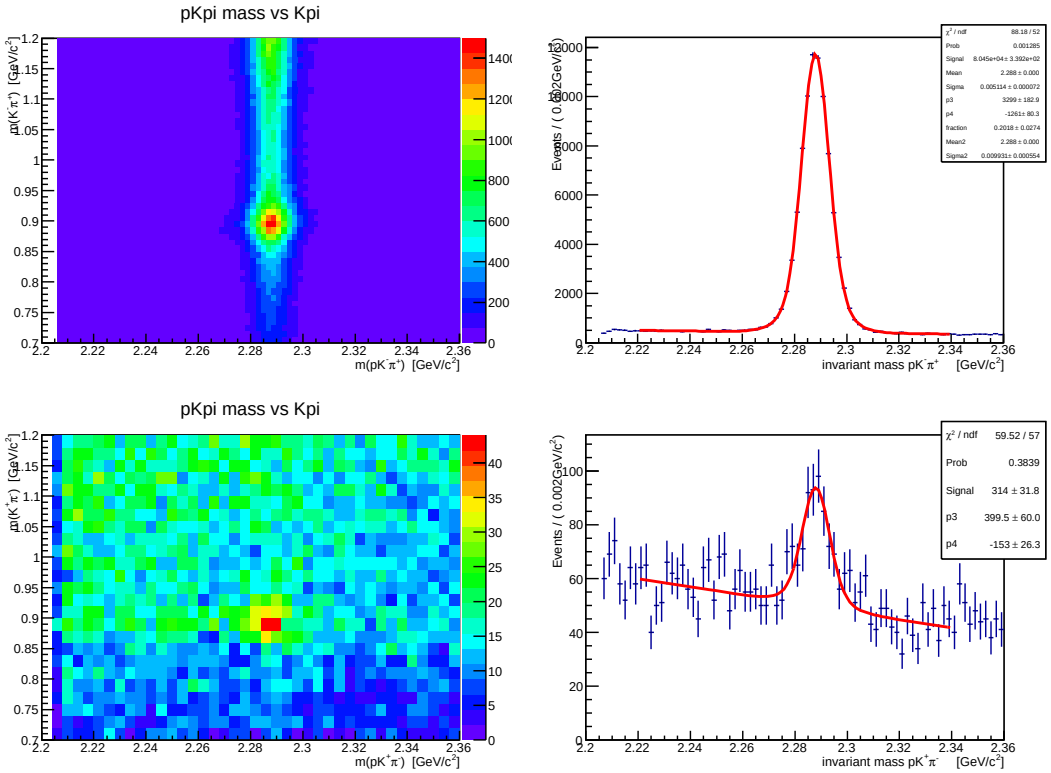

Figure 11: Number of Λ_c decays as function of pKπ invariant mass. The projections on the right are obtained applying a mass cut $0.76 < \mathrm{m(K\pi)/GeV/c^2} < 0.93$.

3.6 Summary of DCS/CF result

Different methods had been used to evaluate systematic error arising from a different reconstruction efficiency for the DCS mode compared to the CF mode, which are summarized in Table 6. Taking the deviations from 1 as systematic error, and adding the different estimates in quadrature, gives an overall systematic error of $\pm 7\%$.

Table 6: Estimates for a correction factor for different reconstruction efficiencies of the DCS and CF mode. † Error taken from the largest deviation from unity in any of the Dalitz plot representations.

method	correction factor
MC Dalitz efficiency weighted by data	0.993 ± 0.007
PID Tables	$0.981 \pm 0.046^\dagger$
p_T distribution	1 ± 0.05

Final results:

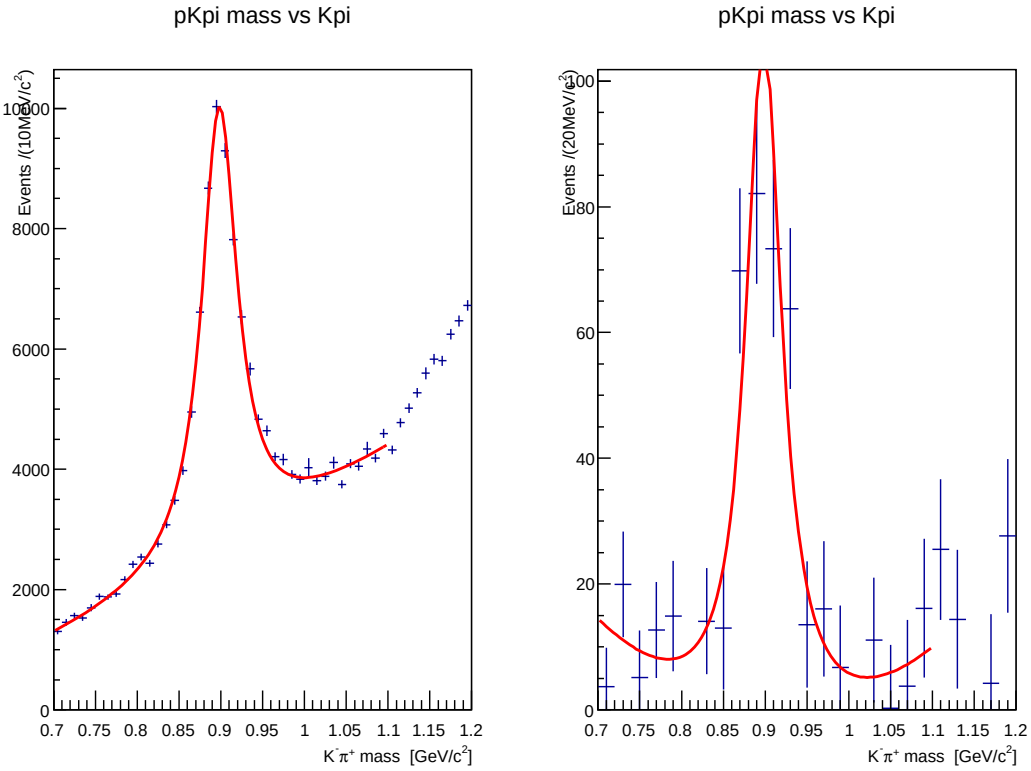

Figure 12: Number of fitted Λ_c events in bins of Kπ invariant mass.

- $BR(\Lambda_c^+ \to pK^+\pi^-)/BR(\Lambda_c^+ \to pK^-\pi^+) = (1.65 \pm 0.18_{stat.} \pm 0.11_{sys.}) \times 10^{-3}$, applying the correction factors of Table6.
- $BR(\Lambda_c^+ \to p\overline{K}^{*0})/BR(\Lambda_c^+ \to pK^{*0}) = (6.79 \pm 0.88 \pm 0.48) \times 10^{-3}$, no correction factors applied, since in same region of Dalitzplot. Being conservative, the same systematic error is being assigned as for the inclusive result.
- $BR(\Lambda_c^+ \to pK^+\pi^-) = (8.2 \pm 0.9_{stat.} \pm 0.6_{sys.} \pm 2.2_{pdg}) \times 10^{-5}$ [1].

[1] Taking the branching ratio of $\Lambda_c^+ \to pK^-\pi^+$ from the PDG, $(5.0 \pm 1.3)\%$

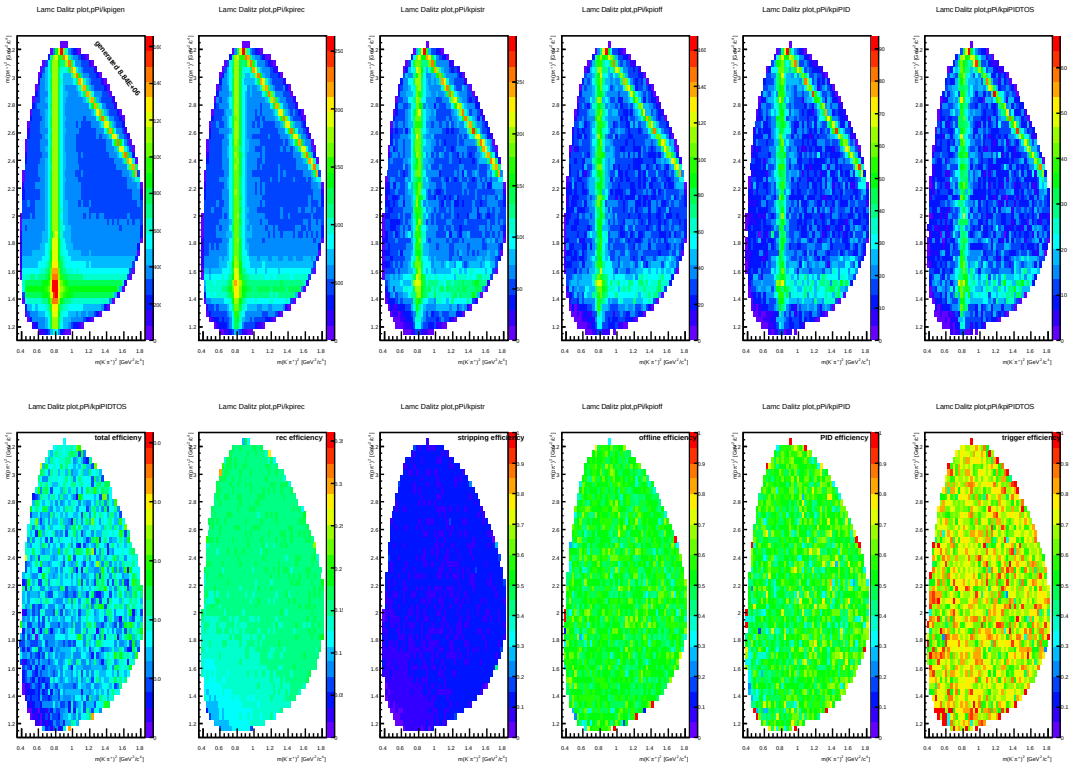

Figure 13: Mean efficiencies in bins of Dalitz plot. Top, from left to right: Generator level, after reconstruction, after stripping, after offline selection, after particle ID, after TOS requirement. Bottom, from left to right: Total efficiency, reconstruction efficiency, stripping efficiency on reconstructed events, offline efficiency, PID efficiency, trigger efficiency.

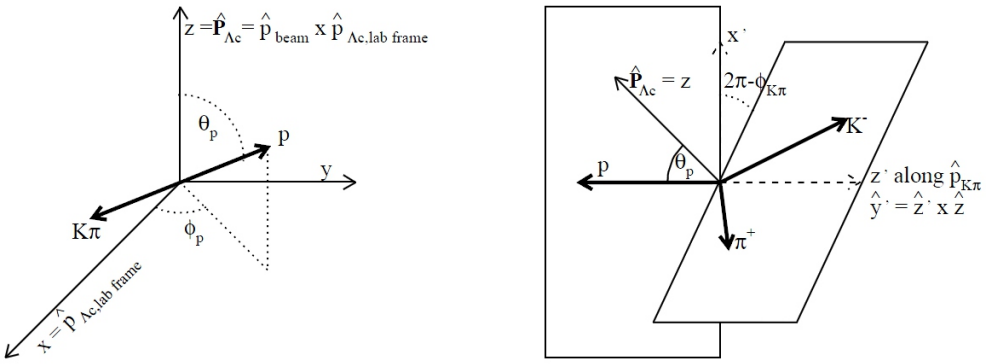

Definition of angles using $\Lambda_c^+ \to p\overline{K}^{*0} \to pK^-\pi^+$ as an example. In both figures the Λ_c^+ is at rest. In the first figure, which defines (θ_p, ϕ_p), the x-axis is along the direction of motion of the Λ_c^+ in the lab frame and the z-axis is the polarization axis, normal to the plane of production. In the second figure we define $\phi_{K\pi}$ as the angle between the plane containing the $\overline{K}^{*0}$ decay products and the plane containing the proton and the x-axis.

Figure 14: Definition of angles as defined by E791[2].

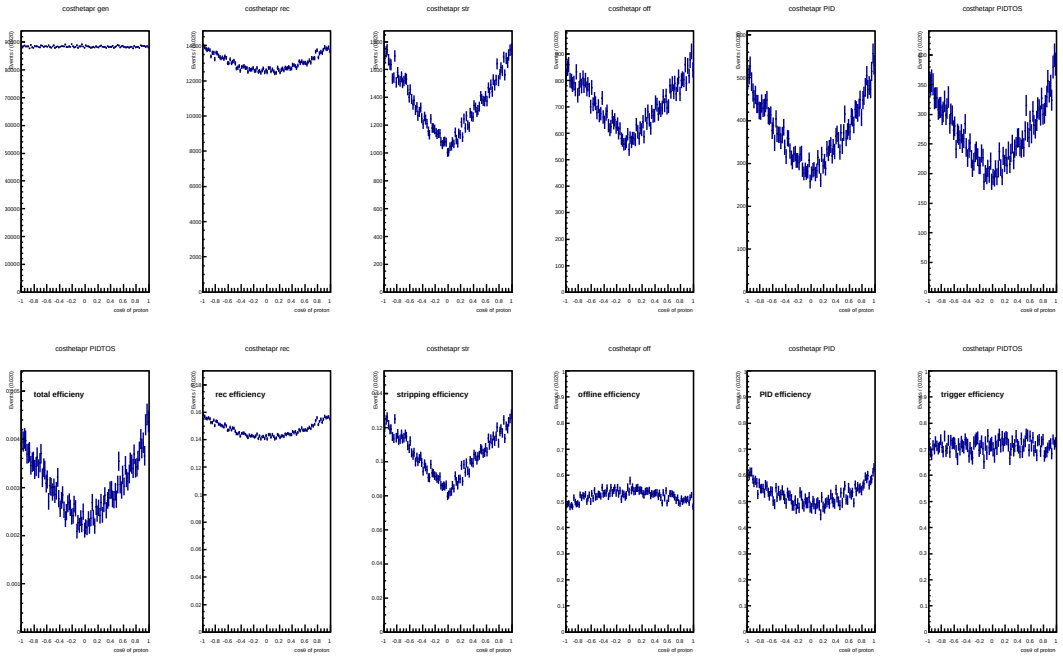

Figure 15: $\cos\theta$ of proton.

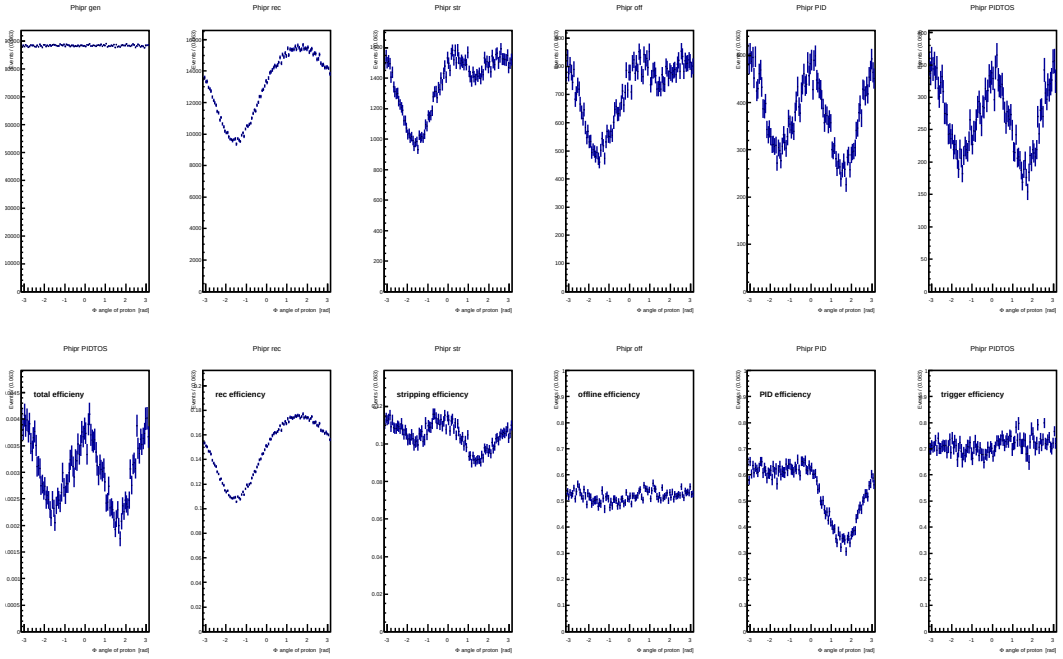

Figure 16: Phi angle of proton.

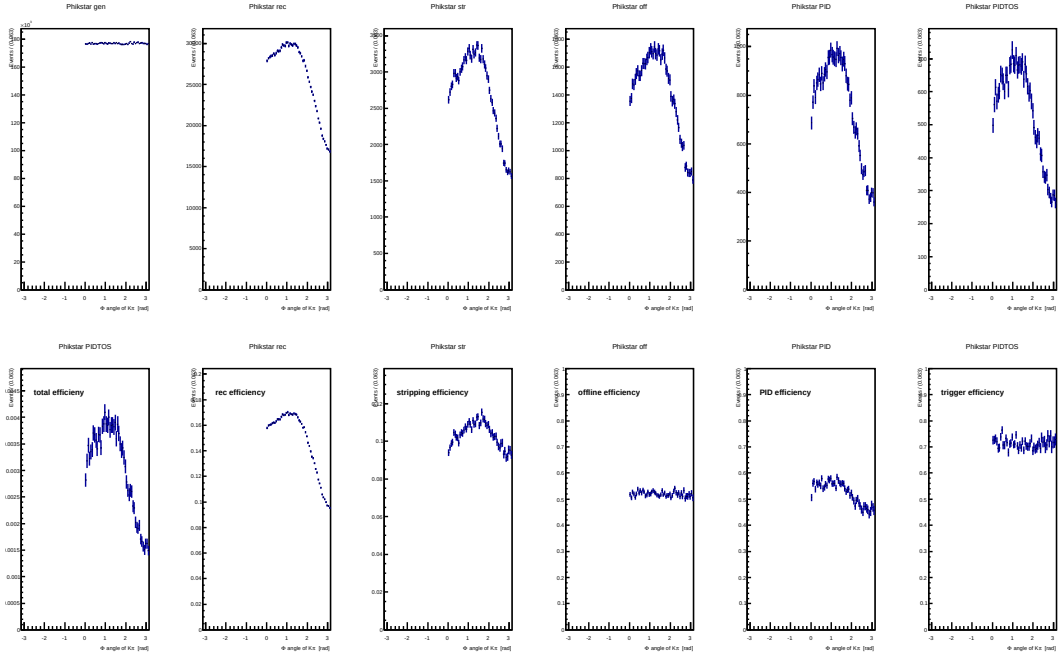

Figure 17: Phi angle of Kπ.

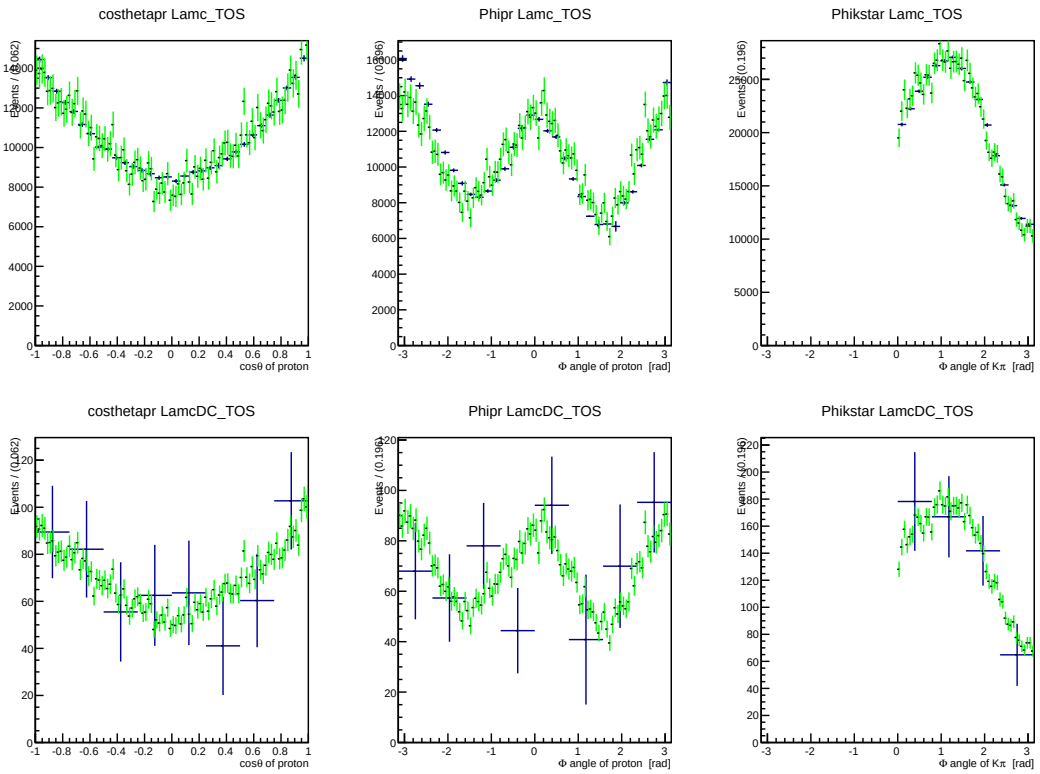

Figure 18: Angular distributions in data compared to MC. Top for the CF mode, and bottom for the DCS mode.

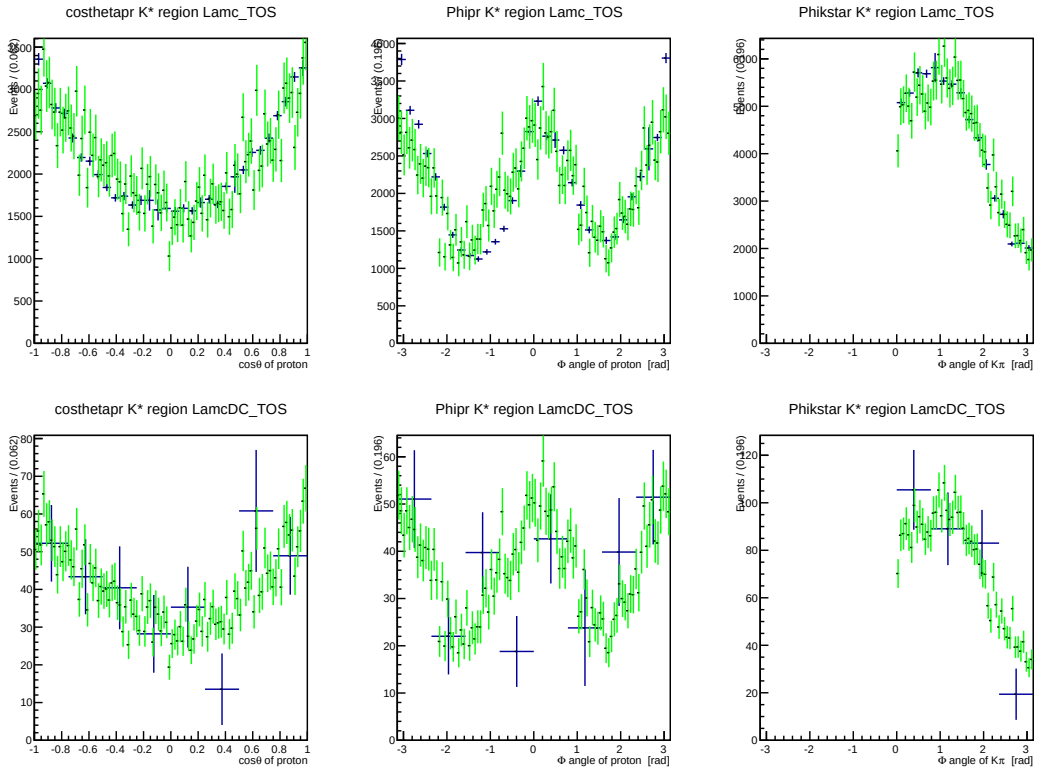

Figure 19: Angular distributions in data compared to MC.

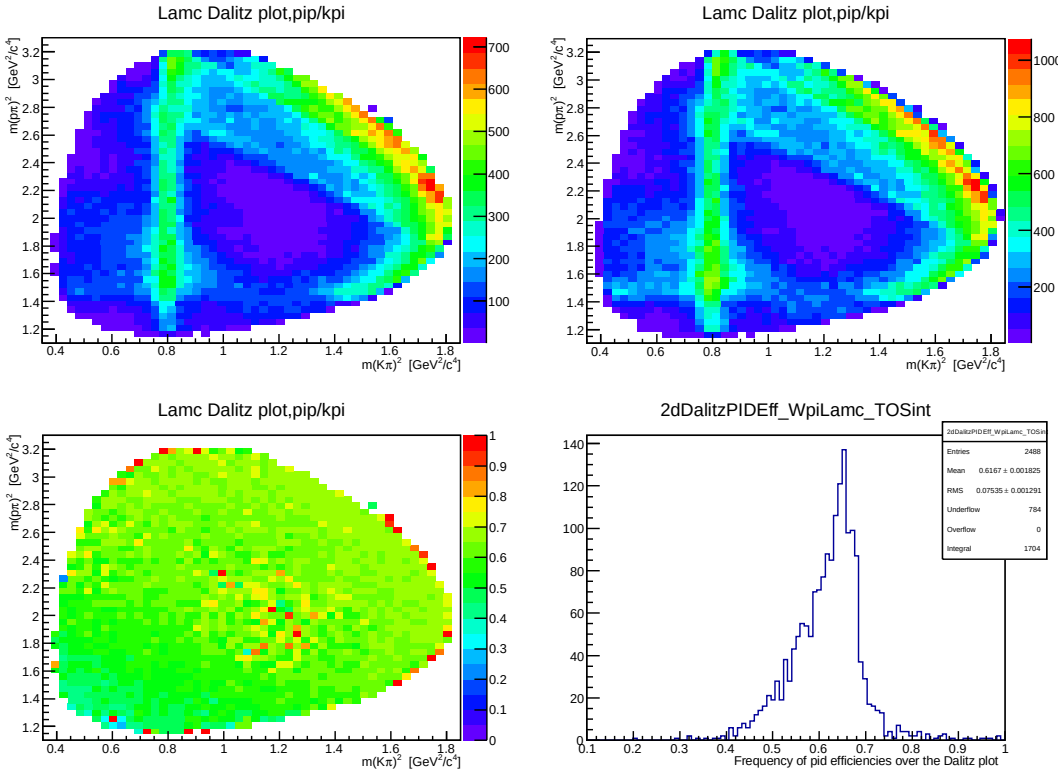

Figure 20: Mean PID efficiencies in bins of Dalitz plot for the CF mode.

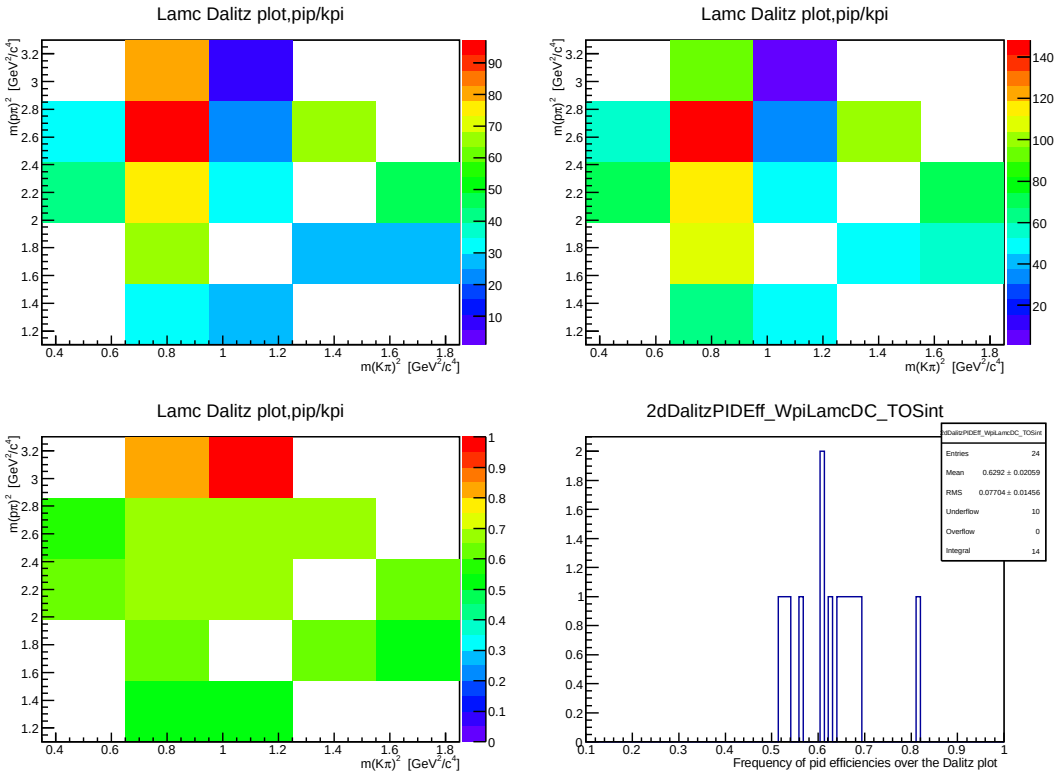

Figure 21: Mean PID efficiencies in bins of Dalitz plot for the DCS mode.

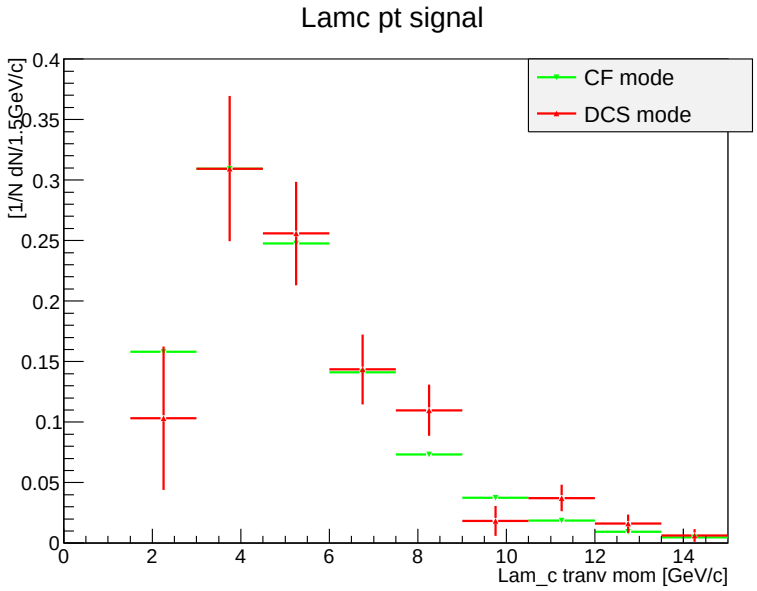

Figure 22: Normalized P_T distribution for the CF and DCS modes.

4 Appendix I

Mass distributions and fits, Fig.23, in different bins of Λ_c p_T. First row: CF, second row: DCS, third row: SCS KK, fourth row: SCS $\pi\pi$.

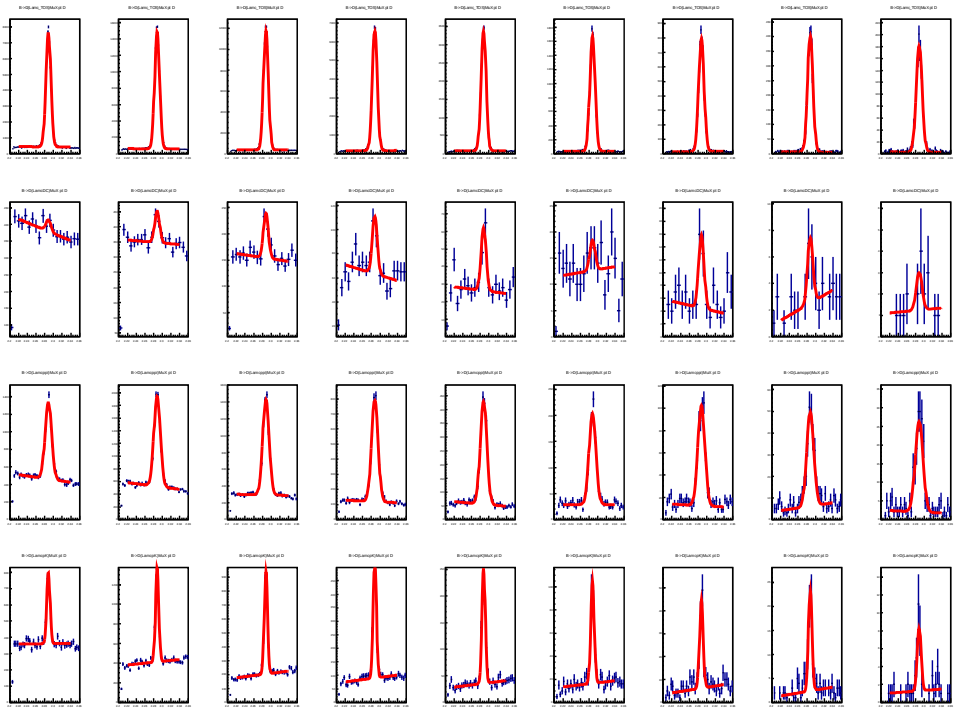

Figure 23: Mass distributions and fits in different bins of Λ_c p_T.

5 Appendix II: Mass fits without TOS requirement

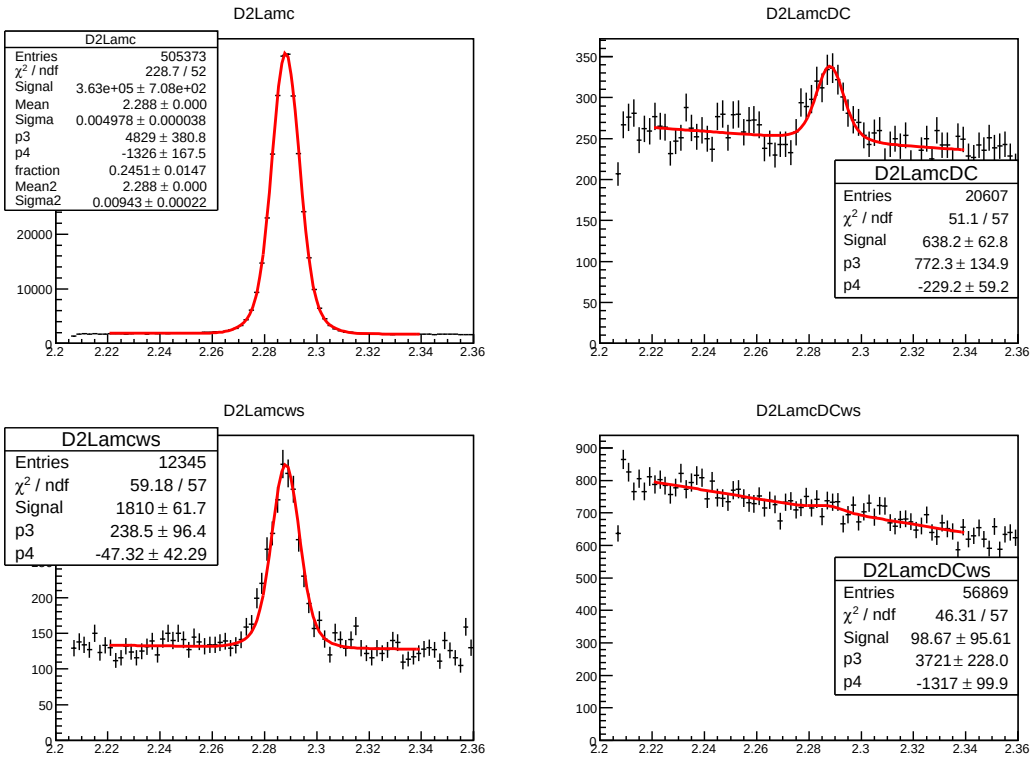

Figure 24: The invariant mass distribution is shown for $pK^-\pi^+\mu^+$, CF, top left, $pK^+\pi^-\mu^+$, DCS, top right, $pK^-\pi^+\mu^-$, CF wrong sign μ, bottom left and $pK^+\pi^-\mu^-$, DCS wrong sign μ, bottom left.

Table 7: Fit parameters of the mass fits separately for magnet up and down, Λ_c^+ and Λ_c^-.

Fit parameter	All	Magnet up	Magnet down	Λ_c^+	Λ_c^-
n_{CF}	362960.0 ± 708.5	150073.7 ± 454.7	212896.0 ± 543.3	178530.6 ± 518.6	184625.4 ± 493.9
$mean_1$	2.28808 ± 0.00002	2.28814 ± 0.00002	2.28803 ± 0.00002	2.28810 ± 0.00002	2.28806 ± 0.00002
$mean_2$	2.28810 ± 0.00007	2.28814 ± 0.00011	2.28807 ± 0.00009	2.28809 ± 0.00013	2.28811 ± 0.00008
σ_1	0.00498 ± 0.00004	0.00498 ± 0.00006	0.00497 ± 0.00005	0.00510 ± 0.00005	0.00486 ± 0.00006
σ_2	0.00943 ± 0.00022	0.00939 ± 0.00034	0.00946 ± 0.00028	0.01034 ± 0.00041	0.00890 ± 0.00024
ratio	0.25 ± 0.01	0.24 ± 0.02	0.25 ± 0.02	0.19 ± 0.02	0.29 ± 0.02
n_{DCS}	638.2 ± 62.8	306.5 ± 40.9	327.8 ± 47.5	283.6 ± 43.2	353.0 ± 45.5
$n_{DCS}/n_{CF}[10^{-3}]$	1.76 ± 0.17	2.04 ± 0.27	1.54 ± 0.22	1.59 ± 0.24	1.91 ± 0.25

6 Appendix III: Fit examples

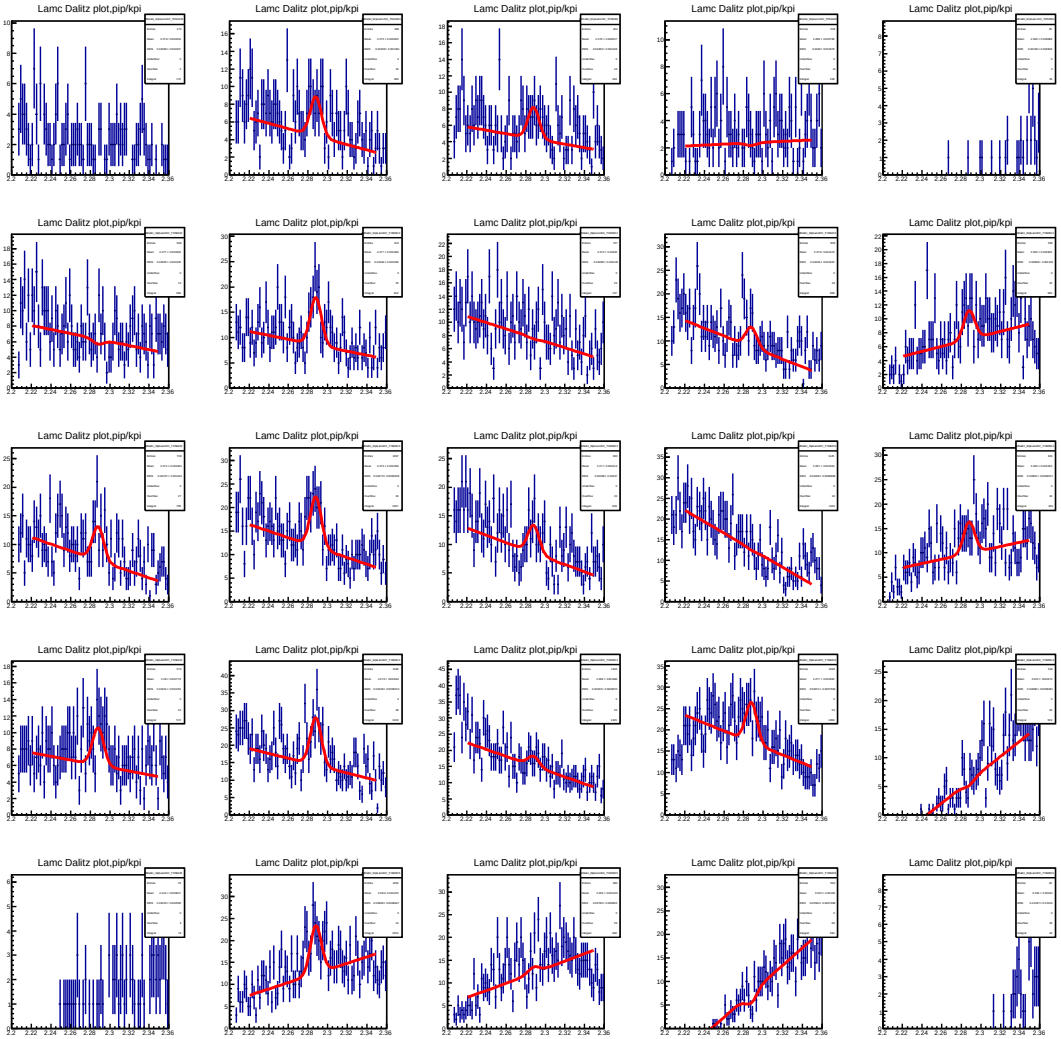

Figure 25: Individual fits for the DCS mode.

7 APPENDIX IV: Event yields for $\Lambda_c \to pK^+K^-$ and $\Lambda_c \to p\pi^+\pi^-$

These results are only shown, since they came out as byproduct of the DCS/CF analysis, and might be of interest for future more detailed studies.

The branching fractions of $\Lambda_c \to pK^+K^-$ and $\Lambda_c \to p\pi^+\pi^-$ are so far only poorly determined. LHCb has large statistics of these decays and could considerably improve the precision. Taking the same cuts as in the DCS analysis, the invariant mass distributions shown in Fig.26 are obtained. The distributions are fitted with a single gaussian and a first order polynomial for the background.

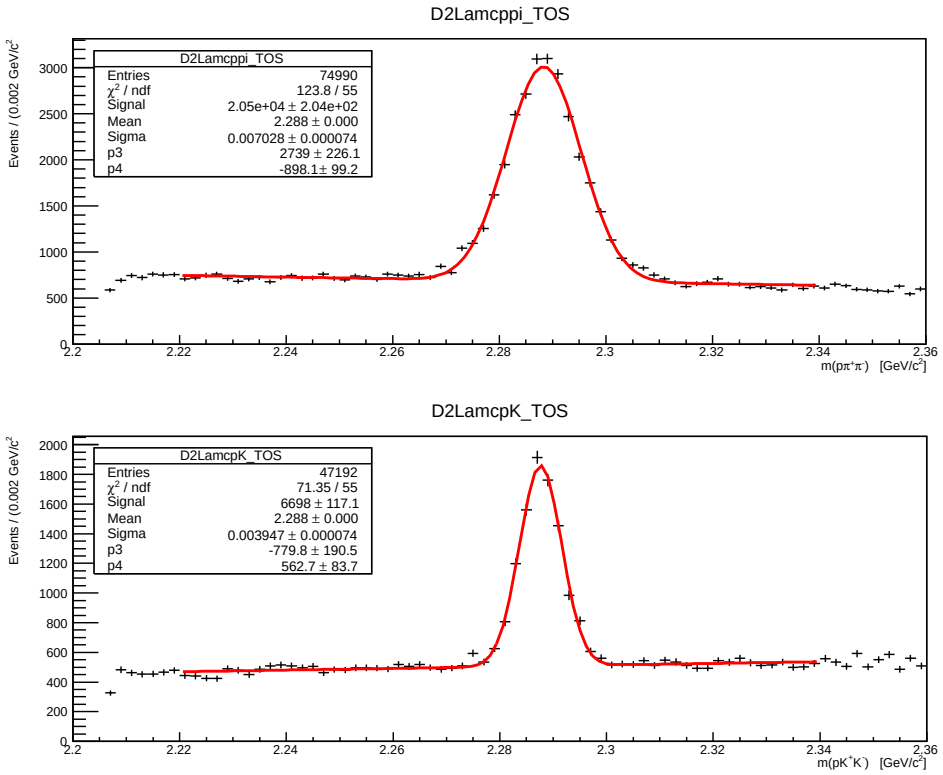

Figure 26: TOS events. The invariant mass distribution is shown for $p\pi^-\pi^+$, top, and pK^+K^-, bottom.

When normalizing to the ${\Lambda_c}^+ \to pK^-\pi^+$mode, differences in the π/K reconstruction needs to be taken into account. A first attempt was made using the PID efficiencies for pions and Kaons from Andrew's tables (Erasmus/PIDCalib) and weight the events with $1/\varepsilon_{K(\pi)} \times \varepsilon_{(K)\pi}$ as function of the track momentum. Fitting the weighted invariant mass distribution and dividing the new event yields by the unweighted event yields gives an idea about the correction factors to be applied, Table 8. In addition, small corrections for acceptance differences and π/K material interaction differences needs to be determined.

Although, the reconstructed p_T distributions, Fig.27, of the Λ_c for the different pHH modes are in reasonable good agreement, indicating that acceptance and reconstruction efficiency differences are small. Adding up only differences which are larger than the statistical error from Fig.27, results in a systematic error of 4% for the p$\pi\pi$ mode and 2.5% for the pKK mode.

The preliminary event yields normalized to the $\Lambda_c \to pK^-\pi^+\mu^+$ channel are given in Table 9.

Table 8: PID correction factor.

mode	f
$\pi\pi$	1.18
KK	0.81

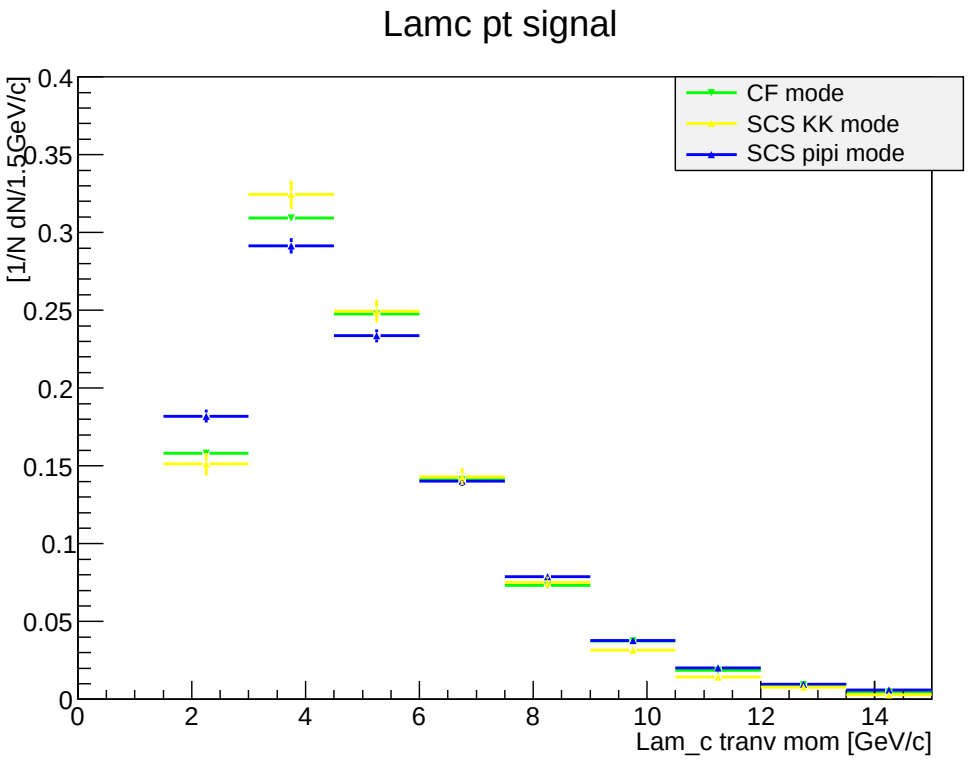

Figure 27: Normalized p_T distributions of the Λ_c in the different pHH modes.

7.1 Dalitz plots

Table 9: Event yields normalized to $\Lambda_c \to pK^-\pi^+$.

mode	uncorrected	PID corrected	PDG
pKK	$(1.99 \pm 0.04)\%$	$(1.62 \pm 0.03)\%$	$(1.5 \pm 0.7)\%$
$p\pi\pi$	$(6.09 \pm 0.06)\%$	$(7.18 \pm 0.07)\%$	$(7 \pm 4)\%$

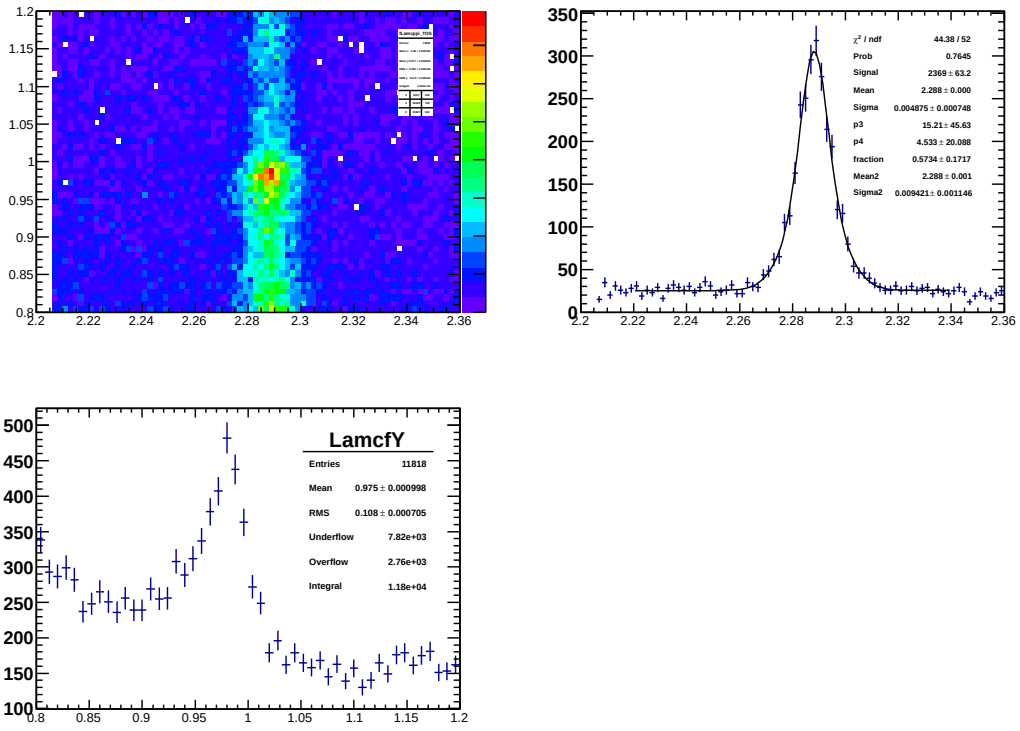

Figure 28: $\pi\pi$ mass versus pKπ showing the f(980) resonance.

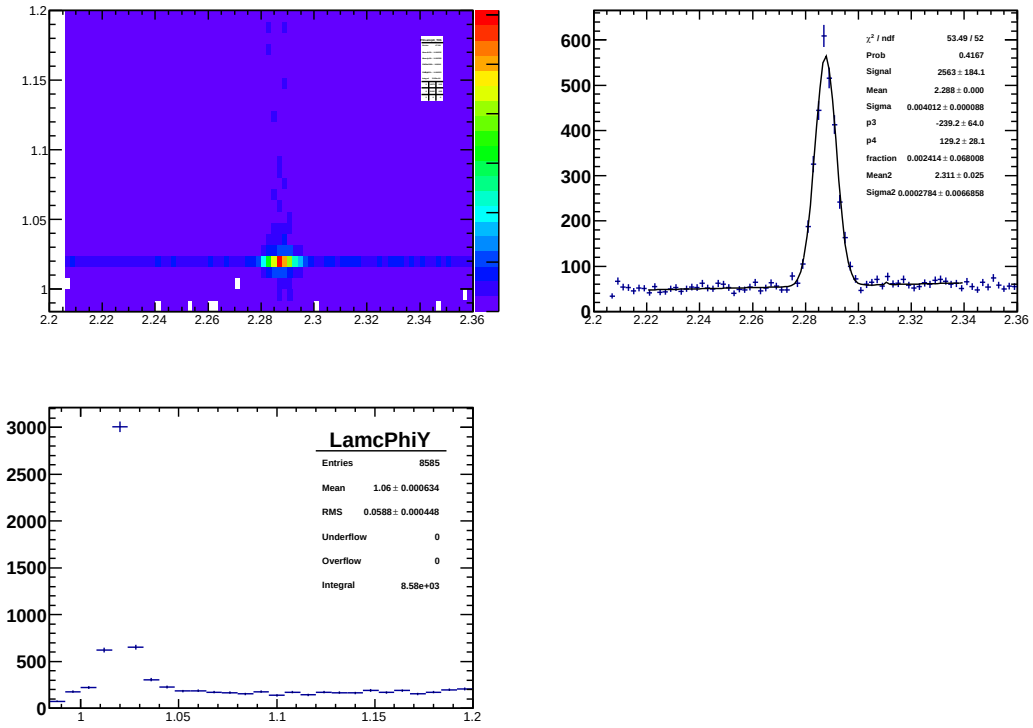

Figure 29: KK mass versus pKπ showing the Φ resonance.

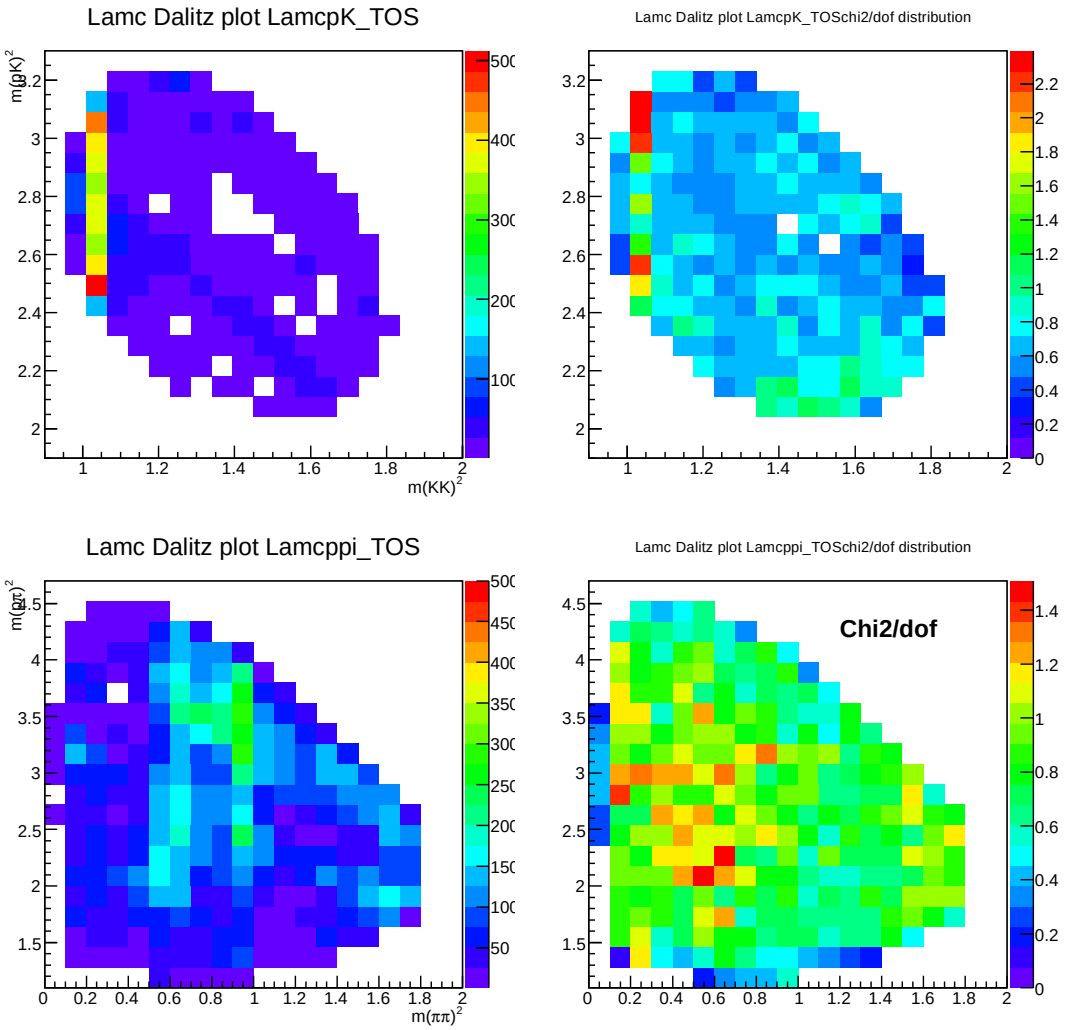

Figure 30: Background subtracted Dalitz plots together with the χ^2 distributions of the signal fits performed in bins of the dalitz plot.

References

[1] LHCb Analysis note ANA-2012-012,
https://twiki.cern.ch/twiki/bin/view/LHCbPhysics/D2hhFromB.

[2] "Multidimensional Resonance Analysis of $\Lambda_c^+ \to pK^-\pi^+$", E791 collaboration, Phys.Lett. B471 (2000) 449-459.

[3] "Individual fits in bins of Dalitz plot for the $\Lambda_c^+ \to pK^-\pi^+$mode",
https://twiki.cern.ch/twiki/pub/LHCbPhysics/Lc2pKpiDCS/LamcIndividualFits.pdf.